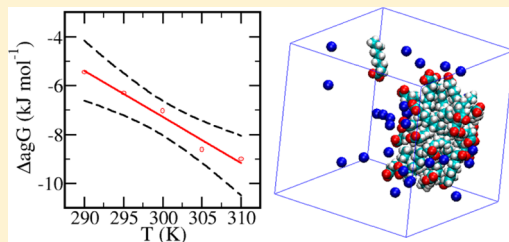


# Aggregation Thermodynamics of Sodium Octanoate Micelles Studied by Means of Molecular Dynamics Simulations

Kalil Bernardino<sup>†</sup> and André F. de Moura<sup>\*,†</sup>

Departamento de Química, Centro de Ciências Exatas e de Tecnologia, Universidade Federal de São Carlos, Rodovia Washington Luiz km 235, CP 676, CEP 13.565-905, São Carlos, São Paulo, Brazil

**ABSTRACT:** The present work is aimed at studying the computation of the thermodynamic potentials that describe the stability of anionic surfactant molecules in micellar aggregates. We report a set of molecular dynamics simulations of a sodium octanoate micelle in aqueous solution using the umbrella sampling method along with the Jarzynski equality in order to compute the potential of mean force for the dissociation process of one surfactant molecule from a previously assembled micellar aggregate. The Jarzynski average was computed at several different temperatures in order to estimate the Gibbs energy of association for the octanoate anion, which was split into its enthalpic and entropic contributions. We also estimated the contributions arising from the polar head and the apolar tail for each thermodynamic potential, and a detailed picture emerged from these simulations. The aggregation is driven mostly by the Gibbs energy contribution arising from the hydrophobic tail, which was large enough to cancel out the unfavorable contribution from the polar head. Although the association process may be ascribed mostly to the transfer of the apolar tail to the micellar core, it should be noted that the polar head also contributed with a favorable entropic term to the overall Gibbs energy. These findings were rationalized by comparing the energetic and structural patterns of the hydration process of a free monomer in solution to an aggregated molecule. The interaction energy distributions presented at least two discernible populations and each population was related to a different structural pattern, as characterized by the radial distribution functions. Altogether, the changes in both the energy and structure of the hydration layer are consistent with the entropy-driven association of the surfactant into the micellar aggregate.



## INTRODUCTION

The driving force for the spontaneous self-assembling of surfactant molecules into organized structures in aqueous solution is usually depicted as a competition between two opposing tendencies, one leading to the decrease of the unfavorable hydrocarbon–water contact and another tending to increase the exposure of the polar headgroups to the aqueous environment. This picture is consistent with the formation of interfaces with oriented molecules, with the heads pointing out to the water solution while their tails remain packed together into an apolar domain. Depending on factors such as molecular size and shape and the degree of repulsion between the surfactant heads, several different microscopic structures may arise other than a bulk phase separation, expected for a nonpolar solute–water system, or the single phase aqueous solution of polar molecules, having several other microheterogeneous structures observed, e.g., micelles, vesicles, and monolayers.<sup>1</sup> Both tendencies are not amenable to exact analytic expressions since the phenomena involved are many body in nature, and it is usual to treat them by means of phenomenological models. On the one hand, the simplicity of the empirical expressions is appealing, somehow explaining why surfactant molecules form stable aggregates in aqueous solution. On the other hand, these empirical models lack details at the molecular level to make them useful to increasing our understanding about which interactions should be assigned as being responsible for driving the aggregation process.

Computer simulations have become standard tools for assessing structural and dynamical information at the molecular level and have been applied in recent years to study the nature of forces involved in micelle formation.<sup>2–9</sup> Although some pieces of information have been obtained using related model systems, e.g., lipid bilayers,<sup>10–12</sup> few if any computational investigations have focused on the molecular level thermodynamic description of micellar aggregation.<sup>13</sup> Indirect results have been published as well, especially regarding the hydrophobic effect, which is responsible for the low solubility of nonpolar solutes in water. It is generally attributed to the entropically unfavorable restructuring of water molecules around a small hydrophobic solute in order to maximize the number of hydrogen bonds between the molecules within the first hydration shell and the surrounding water molecules.<sup>14,15</sup> Below, we present a small survey of recent discussions on aggregation thermodynamics of apolar solutes from the standpoint of computer simulations. Although these and other studies focused on the solvent induced interactions between simple apolar solutes, their conclusions are relevant for the understanding of the hydrophobic effect acting on the surfactant apolar tails.

**Received:** December 29, 2012

**Revised:** May 17, 2013

Primarily, there is an inherent difficulty associated with the estimation of thermodynamic quantities in general, including those describing the hydrophobic effect. For instance, del Rio and Jones<sup>16</sup> showed that the enthalpic contribution to the hydrophobic effect is small due to the fortuitous fact that its signal usually changes near room temperature, although it might become greater than the entropic contribution in some other temperature ranges.

Huang and Chandler<sup>17</sup> showed that the presence of weak attractive van der Waals interactions between a nonpolar solute and water affects the excess chemical potential of the solution but not its temperature dependence for both small solutes and planar hydrophobic surfaces. Thus short-range attraction should affect the enthalpic term of the hydrophobic effect, leaving the entropic contribution unchanged.

Solomonov and Sedov<sup>18</sup> proposed a way to estimate the enthalpy of hydrophobic solvation from experimental measurements for both apolar and amphiphilic solutes. Their main finding was that the hydrophobic solvation enthalpy is negative for alkanes, saturated alcohols, and noble gases whereas it is positive for aromatic hydrocarbons. They also pointed out the fact that hydrophilic and hydrophobic contributions for the hydration enthalpies of alcohols are additive.

Southall et al.<sup>19</sup> studied the hydrophobic effect in two-dimensional simplified model systems by means of Monte Carlo simulations using the Mercedes Benz (MB) water model. If the disk-like solute was small compared to the solvent particles, both the enthalpy and the entropy of the system decreased in cold water, due to the structuring of the water cage around the solute, in agreement with the *iceberg-like* model first proposed by Frank and Evans.<sup>20</sup> On the other hand, solutes at least twice as large as the solvent particles increased the free energy in both hot and cold water by reducing the number of hydrogen bonds between water molecules, increasing the enthalpy without affecting the entropy.

Recently, Lei and Leng<sup>21</sup> calculated the potential of mean force (pmf) between two hydrophobic plates in aqueous solution and showed that the liquid water between the two plates is in a metastable state and that spontaneous drying occurs for distances shorter than a critical value. The solvent structure perturbation was also reported by Maiti et al.,<sup>22</sup> who calculated the pmf between hard sphere solutes at several different temperatures and concluded that the solute perturbation decreased as the temperature increased.

Despite the growing number of computational investigations dedicated to the unraveling of self-assembling mechanisms at the molecular level, including those dedicated to studying the hydrophobic effect, to the best of our knowledge, there has been no computational investigation aimed at the quantitative assessment of the thermodynamic potentials that drive the aggregation of surfactant molecules into micelles. Having identified this gap, we report below the results obtained from a large set of molecular dynamics simulations with the umbrella sampling potential to calculate the Gibbs energy of association of one anionic surfactant in a micellar aggregate. We also report the enthalpy and entropy of association and show how these different thermodynamic potentials may be split into contributions arising from the tail and the head of the amphiphilic molecule. Finally, we also report a detailed analysis of structural patterns that may help us rationalize the solubilization of organic molecules into micelles and related structures, e.g., vesicles, membranes, and Langmuir films.

## METHODOLOGY

The model system consisted of a previously assembled octanoate micelle ( $N = 30$ ) taken from a larger model system.<sup>13</sup> Besides the micellar aggregate, the model system comprised 2500 water molecules and 30 sodium counterions. All molecules were randomly placed in a cubic box, whose edge length was adjusted to yield a density near the experimental value. Strong repulsive contacts were avoided in this initial configuration by means of a minimum cutoff distance between the molecules. The sodium octanoate concentration was ca. 0.7 M, which is about twice the critical micelle concentration (cmc) value for this surfactant and well below the second critical concentration.<sup>23</sup> The proper choice for the surfactant concentration is mandatory for simulations of micellar systems in order to ensure that aggregates remain stable and belong in the correct phase. These requisites were evaluated before any pmf calculation was actually performed, and we found out that the nearly spherical aggregate was stable along a 80 ns molecular dynamics simulation. Being a surfactant with a short aliphatic chain, octanoate anions are expected to be labile and indeed several monomer exchanges were observed within this time scale, resulting in the fluctuation of the aggregation number between 27 and 30 during the simulation. The final equilibrated structure obtained in this simulation, with an  $N = 29$  micelle and a free monomer (Figure 1), was taken as the starting point for the pmf calculations.

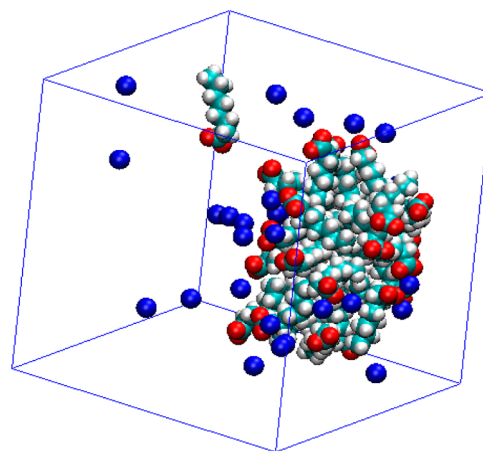


**Figure 1.** Space-filling representation of the initial equilibrated micelle configuration for the umbrella sampling simulations. A randomly chosen octanoate ion was pulled away from the  $N = 29$  micelle. Atoms: oxygen (red), carbon (cyan), hydrogen (light gray), and sodium (blue). The water molecules were omitted for clarity.

In order to obtain the potential of mean force (pmf) corresponding to the aggregation of one octanoate anion into the micelle, we first defined a reaction coordinate beginning at the center of mass of the aggregate and moving radially away from it toward the aqueous solution outside. This is the “so-called” collective variable that defines the association/dissociation process. Of course, the octanoate anion that spontaneously dissociated from the micelle during the equilibration run was not taken into account to define the center of mass of the aggregate, since it cannot be considered to be physically a part of the micelle. Next we chose a random molecule among those comprising the aggregate and defined it as the leaving octanoate anion, which is no longer accounted for in the center of mass calculation. Having defined the

reference group and the leaving molecule, the umbrella sampling may be performed along the reaction coordinate. The procedure consists in the application of a known force in order to keep the leaving molecule around a specified position along the reaction coordinate during the course of a molecular dynamics simulation. A harmonic potential with a force constant of  $1000 \text{ kJ mol}^{-1} \text{ nm}^{-2}$  was applied to keep the head carbon atom (C1) at a nearly fixed distance from the center of mass of the rest of the micelle. The distance from the leaving octanoate C1 atom and the micelle center of mass was changed from an initial distance of 0.9 nm to 2.3 nm at 0.1 nm intervals between consecutive sampling windows. At each window we performed a molecular dynamics simulation, comprising a 0.2 ns relaxation run followed by a 1.0 ns production simulation. The radial distribution function obtained from these simulations was biased due to the harmonic potential  $U(r)$ , yielding  $g^{\text{bias}}(r)$ , from which the unbiased distribution  $g(r)$  may be obtained by the proper removal of the harmonic potential bias (eq 1),<sup>24</sup> where  $r$  is the distance between the micelle center of mass and the head carbon from the leaving octanoate.

$$g(r) = g^{\text{bias}}(r) - e^{-U(r)/RT} \quad (1)$$

The radial distribution function  $g(r)$  may be defined as the ratio between the average density of type A particles around type B reference particles within a spherical shell of radius  $r$  and thickness  $dr$  and the average density of type A particles in the whole system (eq 2).<sup>25</sup> A similar definition holds for the biased radial distribution function  $g^{\text{bias}}(r)$ , which is defined in terms of the density values for the system in the presence of the harmonic potential  $U(r)$ .

$$g(r) = \frac{\rho_{\text{AB}}(r)}{\rho_{\text{A,system}}} \quad (2)$$

The unbiased potential of mean force may be derived from the combination of the distributions from each umbrella sampling window (with the center of the harmonic potential in a different distance  $r$  along the reaction coordinate) using the weighted histogram analysis method (WHAM).<sup>26–29</sup>

The umbrella sampling method should be regarded as a way of obtaining the pmf at thermodynamic equilibrium as long as the phase space is thoroughly sampled and the bias is properly removed using, for instance, the WHAM procedure. In this case, the reversible pmf is given by eq 3.<sup>25</sup>

$$\text{pmf}(r) = -RT \ln[g(r)] \quad (3)$$

Thorough sampling is particularly important for small systems, due to the large structural and energetic fluctuations that may be observed even for an equilibrated system. For instance, the sodium octanoate micellar system under investigation may have structural and energetic fluctuations associated with physical phenomena as diverse as the association/dissociation of  $\text{Na}^+$  ions at the interfacial region and the conformational changes of the aliphatic tails, as well as the accompanying hydration changes associated with both phenomena, as discussed under Results and Discussion.

In practical terms, the time expended at each umbrella sampling window should be large when compared to the relaxation times of the system, in order to guarantee the equilibration of the radial distribution function  $g(r)$ . Obviously, infinite sampling is not feasible; therefore the length of the simulation at each sampling window should be checked for

convergence of the calculated pmf. Unfortunately, the sodium octanoate micellar system poses one sound physical reason why the sampling to improve accuracy should not be increased: monomer exchange and even micelle breakup may be very often observed if the simulation exceeds a few nanoseconds, due to the short aliphatic chain of octanoate anions. From a purely technical standpoint, the aggregate could be stabilized by an extra harmonic potential, which would hold together the surfactant molecules around a specified center of mass, but this artificial interaction would most likely introduce artifacts, since the octanoate micelle presents oscillating values for both the radius of gyration and for the components of the moment of inertia (results not shown here). Obviously, any ad hoc interaction would affect both the structure and the dynamics of the aggregate, which in turn would introduce an unknown bias in the calculated thermodynamic potentials.

In order to ensure the stability of the aggregate during the sampling, a limit for the simulation, at each sampling window along the reaction coordinate, has been chosen (a short relaxation run followed by a 1.0 ns sampling run). On the one hand, this time scale was short enough to ensure the stability of the micellar aggregate, but on the other hand, it was not long enough to obtain an equilibrated pmf, since different umbrella sampling simulations with the same setup yielded different pmf profiles. Therefore, we must now turn our attention to the averaging of a small set of independent pmf profiles obtained from short umbrella sampling simulations.

We performed six umbrella sampling simulations for each temperature, pulling a different octanoate anion from the micelle for each simulation. Each one of these umbrella sampling runs yielded an unbiased distribution  $g_i(r)$  and a corresponding pmf (eq 4), which should not be regarded as an equilibrium profile for any individual run.

$$\text{pmf}_i(r) = -RT \ln[g_i(r)], \quad i = 1, 2, \dots, n \quad (4)$$

The independent distributions  $g_i(r)$  may be combined into the distribution  $g(r)$  by simple arithmetic average (eq 5), which should become equal to an equilibrium umbrella sampling distribution within the limit of  $n$ , approaching infinity.<sup>25</sup>

$$g(r) = \frac{1}{n} \sum_{i=1}^n g_i(r) \quad (5)$$

The substitution of eqs 4 and 5 into eq 3 yields the correct expression of combining  $n$  different pmf profiles, each one derived from a distribution with insufficient sampling, in an averaged profile (eq 6), which should be regarded as an estimate of the true equilibrium pmf.

$$\text{pmf}(r) = -RT \ln \left[ \frac{1}{n} \sum_{i=1}^n \exp \left( \frac{-\text{pmf}_i(r)}{RT} \right) \right] \quad (6)$$

This expression is a particular case of the Jarzynski equality,<sup>29</sup> which is most often used to estimate the free energy of any given process as an average of the measured/calculated amounts of work done along a large number of irreversible paths. As we have demonstrated here, the Jarzynski equality also holds for the combination of a set of independent pmf profiles obtained using an equilibrium methodology but lacking proper convergence due to poor sampling issues, and eq 6 should be used instead of a simple arithmetic average. Although this demonstration should not be taken as a proof of the Jarzynski equality, we demonstrated that this is the correct way



to cancel statistical errors while averaging an independent set of pmf profiles.

Whether the pmf was obtained by a set of independent runs using eq 6 or by only one equilibrium run using eqs 1 and 3, when a radial distribution function is used to calculate the pmf a further correction of  $-2RT \ln(r/r_0)$  is needed in order to take into account the entropic contribution arising from the rotation of the two groups,<sup>30,31</sup> where  $r_0$  is the position taken as the reference state of the pmf profile, which was chosen to be the farthest radial distance in all umbrella sampling calculations,  $r_0 = 2.3$  nm. This correction was applied to all the pmf profiles presented in this paper.

In order to obtain the enthalpy and entropy of aggregation, the potential of mean force was calculated at five different temperatures: 290, 295, 300, 305, and 310 K. Assuming that this temperature range is narrow enough for the enthalpy and entropy of aggregation to be considered constants, these quantities may be derived straightforwardly from the linear regression of the Gibbs energy of aggregation as a function of the temperature. The Gibbs energy of association is defined as the minimum value obtained for the potential of mean force, setting the reference zero value for all pmf curves at 2.3 nm.

The Gibbs energy of association and its enthalpy and entropy terms can be separated into contributions arising from the polar headgroup and the hydrophobic tail. This alchemical splitting can be accomplished by means of the pmf calculation for a molecular fragment that is representative of either the head or the tail, assuming that all state functions we are dealing with are additive. We have previously demonstrated that the first methylene group attached to the carboxylate moiety behaves as a polar group, even though its atoms are typically apolar in the force-field description.<sup>13</sup> This behavior had already been reported in experimental investigations and is usually described as an electrorestriction effect.<sup>25</sup> Bearing in mind this unique characteristic of the first methylene group, the octanoate molecule should be split into a hexane-like tail and an acetate-like head. Either one of these fragments would have to be saturated with an extra hydrogen atom to fill the fourth carbon chemical bond, which was broken to build these fragments. Although this extra atom breaks the exact equivalence between the fragments and the whole molecule, we consider this small topological difference to be a better option compared to the simulation of ill-defined chemical species that would most likely introduce artifacts. Consistent with all these reasonings, we chose the molecular fragment to be the acetate anion and we performed pmf calculations along the same reaction coordinate that we defined for the removal of the octanoate anion, calculating the Jarzynski average for four different pmf curves in each temperature (pmf calculations were highly reproducible in this case, being sufficient to calculate only four replicas in order to obtain a reliable average curve). Each pmf calculation started with the conversion of one randomly chosen octanoate anion of the micelle into an acetate anion by replacing the tail fragment ( $C_6H_{13}$ ) by a hydrogen atom.

Besides performing an extensive set of umbrella sampling simulations to compute the Gibbs energy of association and its components, we also performed a 20-ns-long molecular dynamics simulation to calculate energetic and structural properties of the system that may give us some insight into the molecular basis of the calculated thermodynamic potentials. The simulation was carried out keeping in the solution the octanoate monomer that had been pulled away during one of the umbrella sampling runs by means of a quadratic potential

with a force constant of  $250 \text{ kJ mol}^{-1} \text{ nm}^{-2}$ . This smaller force constant was used here only to avoid the return of this ion to the micelle. This choice, although arbitrary, makes the comparisons easier, since this aggregation number ( $N = 28$ ) was observed throughout the umbrella sampling calculations (besides the monomer restricted by the force constant, a second monomer was also present in the solution in the start of this simulation but it was spontaneously incorporated into the micelle during the run).

All simulations were performed using the GROMACS 4.0.5 package.<sup>32–34</sup> The interactions were described using the OPLS-AA force field<sup>35</sup> for octanoate and acetate anions, Åqvist's parameters<sup>36</sup> for sodium counterions, and the SPC model<sup>37</sup> for water. The nonbonded interactions were truncated at 1.5 nm, using the particle mesh Ewald (PME) method<sup>38,39</sup> to treat the long-range electrostatic potential beyond the cutoff distance and a shift function for the Lennard-Jones interactions. An integration time step of 1.0 fs was used in all simulations. The weak coupling scheme of Berendsen<sup>40</sup> was used for both the temperature ( $T = 300$  K for the equilibrium simulations and 290, 295, 300, 305, and 310 K in the umbrella sampling runs,  $\tau_T = 0.1$  ps) and the pressure ( $p = 1$  bar,  $\tau_p = 1.0$  ps and  $\kappa = 4.5 \times 10^{-5} \text{ bar}^{-1}$ ). VMD 1.8.7<sup>41</sup> was used to visualize the trajectories and to render the graphical representations of the system.

## RESULTS AND DISCUSSION

**Potential of Mean Force and Thermodynamics of Aggregation of Sodium Octanoate.** The potential of mean force, for the case of an association process, is the amount of thermodynamic work that is necessary to bring two particles from the dissociated state to the aggregated state in a condensed medium, being equal to the Gibbs energy difference between these states if the work is performed reversibly. Checking each umbrella sampling simulation to ensure that the physical process of interest was indeed observed is mandatory, since other unforeseen processes may happen as well and since the resulting Gibbs energy is now a combined value for the overall process and cannot be easily split into separate contributions for each individual process. For instance, it must be verified whether the micelle remained whole along the umbrella sampling simulation, as well as the number of surfactant molecules that actually left the micellar aggregate (sometimes a second molecule leaves the aggregate along with the pulled molecule, usually due to the presence of a sodium ionic bridge between the two octanoate anions).

Taking the distance between one octanoate head carbon and the center of mass of the rest of the micelle as the reaction coordinate, we observed a wide variety of pmf profiles, most of them with the minimum at a distance shorter than 1.5 nm (Figure 2). The pmf curves presented local fluctuations and even activation barriers, depending on the local chemical environment being sampled. The Jarzynski equality (eq 6) always favors the most negative values among the independent replicas at each position of the reaction coordinate, and the resulting averages are smoother than the raw data for all temperatures, with a minimum at the surface of the micelle (ca. 1.3–1.4 nm). The oscillations and the activation barriers of passing from the micelle surface to the aqueous solution should be regarded as transient profiles of a single observation, whereas any thermodynamic observation should be regarded as an average over a huge number of observations. The Jarzynski average captures this long-term behavior and damps the oscillations while keeping the main features of the process.

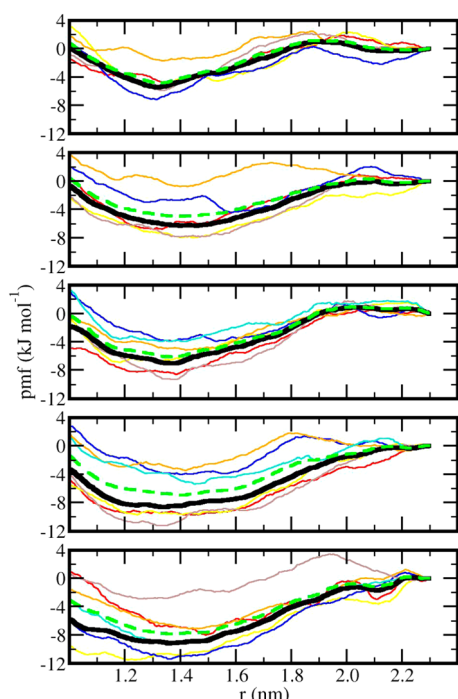


**Figure 2.** Potential of mean force for the removal of one octanoate anion from the micelle at five different temperatures (from top to bottom: 290, 295, 300, 305, and 310 K). The bold black curve is the Jarzynski average (eq 6) calculated from the pmf curves, the dashed green curve is the arithmetic average, and the other colors stand for independent umbrella sampling simulations.

One important feature that is expected for a dissociation process in general is the formation of a pmf plateau at large distances, which is observed for the averages, although many individual pmf curves do not present well-defined plateaus in the aqueous solution. The formation of a pmf plateau before the largest distance in our reaction coordinate is reached means that setting the reference state at  $r = 2.3$  nm, although arbitrary, is physically meaningful.

Although our analysis will rely mostly on the averaged pmf, it is worth noting the variety of processes that may take place when a single association event is considered. For instance, large differences in Gibbs energy of association reflect, among other factors, the fluctuations in sodium concentration at the interface region. Another interesting finding about the individual processes is the fact that some of the pmf curves either form shallow negative minima or remain positive along the whole association coordinate. This is consistent with the observation that octanoate anions are labile and monomer exchanges are observed quite often after tens of nanoseconds.<sup>13</sup> The arithmetic average of the individual pmf curves for each temperature is also presented in Figure 2 for comparison purposes. The difference between the arithmetic averages and those obtained by means of the Jarzynski equality is small, with the latter being always slightly less negative than the former. This is a known issue for the application of the Jarzynski equality to a small number of independent replicas, since, even though rarely, a pmf value may lie well below the actual average and consequently give a large contribution to the calculated average, due to the use of exponential factors of  $-\text{pmf}_i/RT$  in eq 6.<sup>29</sup> As we have already discussed under Methodology, the use of eq 6 should be regarded as the correct procedure to average these sets of independent pmf profiles, and therefore,

from now on, only the averages obtained by means of the Jarzynski equality will be used in the following discussions.

One pmf curve at 290 K had to be discarded due to the fortuitous removal of a second octanoate ion together with the pulled one. This event happened only during this pulling, and we could no longer characterize the process as the removal of one, and only one, octanoate anion from the micelle. This second octanoate resulted in a deeper minimum for the pmf ( $-11.5 \text{ kJ mol}^{-1}$ ), which would amount to a reduction of ca.  $2.4 \text{ kJ mol}^{-1}$  in the average Gibbs energy of association. One pmf at 295 K also had to be discarded due to the formation of a dimer between the pulled octanoate and the monomer initially present in the solution after the pulled octanoate left the micelle. Although the excluded curve was not significantly different from the other curves, we considered that a different final state for the octanoate, which ended up as a dimer instead of a monomer, was a sound physical reason to disregard this simulation as well. These excluded curves were not included in Figure 2.

The precision of our estimates for the Gibbs energy of association may be conveniently assessed by recalculating the Jarzynski averages presented in Figure 2 without either the most negative curve or the most positive one. In both cases the differences amounted to less than  $1.0 \text{ kJ mol}^{-1}$  at the minimum pmf for all temperatures that were considered in our study. We shall consider this figure to be the precision of the values to be presented and discussed in the following sections.

We also performed a set of pmf calculations for an acetate anion along the same reaction coordinate and at the same temperatures in which the octanoate removal was investigated (Figure 3). The acetate anion is a model fragment for the

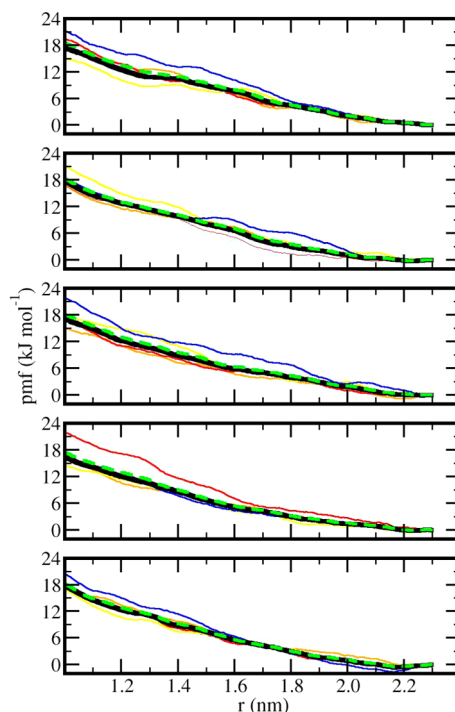


**Figure 3.** Potential of mean force for the removal of one acetate anion from the micelle at five different temperatures (from top to bottom: 290, 295, 300, 305, and 310 K). The bold black curve is the Jarzynski average (eq 6) calculated from the pmf curves, the dashed green curve is the arithmetic average, and the other colors stand for independent umbrella sampling simulations.

carboxylate polar head, and it behaves as expected for ionic species, with a lower Gibbs energy in the aqueous solution than inside the apolar micellar core. Although the pmf plateaus for the acetate anion at the end of the reaction coordinate are not as well-defined as those obtained for the octanoate anion, we have set all pmf curves to the same reference state at 2.3 nm and have defined the Gibbs energy of aggregation of the acetate ion by the averaged pmf value at the distance of  $r$ , corresponding to the minimum for the octanoate at the same temperature.

The contribution arising from the tail can be estimated as the difference between the Gibbs energy of association for the octanoate anion and that for the acetate anion, assuming the additivity of the contributions arising from each fragment. From a strictly formal point of view, the Gibbs energy for any transfer process cannot be partitioned as an exact sum of contributions for the constituent molecular fragments, but it is accepted on empirical grounds that only minor errors are introduced by the additivity hypothesis. For instance, the solubility properties of a molecule can be predicted by several empirical parameters which are computed using tabulated thermodynamic parameters for molecular fragments, e.g., the hydrophilic–lipophilic balance (HLB) and the solubility parameter. For instance, the HLB for a molecule may be computed as the difference between the sum of contributions arising from hydrophilic groups and the sum of contributions arising from hydrophobic groups.<sup>42,43</sup> As regards the precision of the computed estimates with respect to the actual solubility properties, the additivity hypothesis typically introduces an error below 10% for the solubility parameter compared to experimental data.<sup>43</sup>

The additivity hypothesis also plays an important role in the micellization thermodynamics of surfactant molecules. For instance, the logarithm of the critical micelle concentration (cmc) varies linearly with the number of carbon atoms ( $n_C$ ) comprising the hydrophobic tail (eq 7).<sup>43,44</sup> The empirical parameters  $A$  and  $B$  are positive constants that depend exclusively on the temperature and the chemical nature of the surfactant head, and on the counterion identity for the case of ionic surfactants.

$$\ln(\text{cmc}) = A - Bn_C \quad (7)$$

This empirical relation may be combined with the standard thermodynamic result relating the Gibbs energy of aggregation and the logarithm of the cmc (eq 8),<sup>43–45</sup> yielding a linear relation between the Gibbs energy of aggregation and the number of carbon atoms comprising the hydrophobic tail (eq 9). Altogether, these theoretical and experimental results lend support to the additivity of the thermodynamic potential describing the aggregation of the octanoate anion in the micelle in terms of the contributions arising from the polar head and the apolar tail.

$$\Delta G_{\text{ag}} = RT \ln(\text{cmc}) \quad (8)$$

$$\Delta G_{\text{ag}} = RTA - RTBn_C \quad (9)$$

The entropy and the enthalpy of aggregation and the fragment contributions were estimated by assuming that their values were constant in the narrow temperature range under consideration, allowing the direct comparison of the linear regression coefficients obtained for the Gibbs energy as a function of the absolute temperature (Figure 4) with the fundamental thermodynamic relation for the aggregation process (eq 10).

$$\Delta_{\text{ag}}G = \Delta_{\text{ag}}H - T\Delta_{\text{ag}}S \quad (10)$$

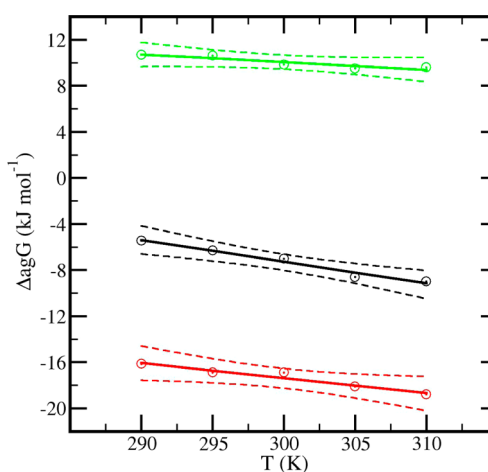


**Figure 4.** Gibbs energy of aggregation for the octanoate anion. (black open circles) Octanoate anion (whole molecule); (red open circles) apolar tail contribution; (green open circles) polar head contribution. The solid lines stand for the linear regression models, whereas the dashed lines stand for the 99% confidence bands.

The squared correlation coefficient  $R^2$  for the linear regressions was of 0.98 for the octanoate anion, 0.86 for the polar head, and 0.91 for the apolar tail. Of course, the regressions could be improved by a more thorough sampling, e.g., by increasing the number of replicas in the Jarzynski equality, but we consider the present data set to be adequate, since all the points fall within the 99% confidence bands.

All the thermodynamic properties are summarized in Table 1. These regression estimates and the raw data in Figure 4 give

**Table 1. Summary of the Thermodynamic Potentials Derived from the Linear Regression Coefficients for the Gibbs Energy as a Function of Temperature**

thermodyn contrib	octanoate	polar head	apolar tail
$\Delta_{\text{ag}}H$ (kJ mol <sup>−1</sup> )	51 ± 5	30 ± 5	21 ± 7
$\Delta_{\text{ag}}S$ (J K <sup>−1</sup> mol <sup>−1</sup> )	194 ± 18	66 ± 15	128 ± 23
$-T\Delta_{\text{ag}}S$ (at 300 K (kJ mol <sup>−1</sup> ))	−58 ± 5	−20 ± 4	−38 ± 7

a quantitative picture of the thermodynamic driving forces involved in the self-assembling of this anionic surfactant. The first thing to note is the fact that the polar head and apolar tail have opposite roles in the aggregation process, as expected, with the former yielding an unfavorable contribution to the Gibbs energy of association, whereas the latter yielded a favorable and larger contribution. These contributions add up into an overall favorable Gibbs energy for the association of the monomer into the micellar aggregate. The aggregation is usually thought of as an entropy-driven process, and the regression confirms this hypothesis, yielding favorable entropic terms for both the polar head and the apolar tail. The hydrophobic effect for an apolar tail may be ascribed to the ordering of water molecules around the solute, forming a cage that is disrupted during aggregation, releasing water molecules from this orderly arrangement back to the bulk solvent.<sup>20</sup> With regard to the favorable entropic contribution arising from the polar head, the  $-T\Delta_{\text{ag}}S$  contribution at 300 K is larger than the



overall Gibbs energy of aggregation at the same temperature ( $-7.0 \text{ kJ mol}^{-1}$ ), meaning that the aggregation process of small surfactant ions probably would not be thermodynamically favorable without this contribution, a result that, to the best of our knowledge, has not been reported or even suggested in the literature yet. Further analysis needs to be performed to shed some light on the structural features that might be responsible for the aggregation driving forces. These analyses will be reported in the sections Structural and Energetic Analysis of the Surfactant Polar Head upon Aggregation and Contributions Arising from the Hydrophobic Tail.

The Gibbs energy of association for the apolar tail yielded  $-2.8 \text{ kJ mol}^{-1}$  per  $\text{CH}_2/\text{CH}_3$  group, in good agreement with the estimated Gibbs energy of transfer of linear alkanes from water solution into the bulk liquid hydrocarbon, which amounts to  $-3.8 \text{ kJ mol}^{-1}$  per  $\text{CH}_2/\text{CH}_3$  group.<sup>14</sup> Considering the differences between a bulk phase separation and an aliphatic tail attached to a polar headgroup and packed inside a small micelle, the agreement should be considered sufficiently good. The Gibbs energy of aggregation per  $\text{CH}_2/\text{CH}_3$  segment can be computed using eq 9 with the tabulated empirical values for the constants *A* and *B* for sodium carboxylates.<sup>44</sup> The resulting relation yields  $-2.0 \text{ kJ mol}^{-1}$  per  $\text{CH}_2/\text{CH}_3$  group at 300 K, confirming that our estimate should be considered reliable.

**Structural and Energetic Analysis of the Surfactant Polar Head upon Aggregation.** The most obvious reason why the enthalpy of aggregation is positive for the whole molecule as well as for the head contribution is the fact that the octanoate is a negatively charged surfactant, and micellization brings all the negatively charged heads into contact. The repulsive energy contribution between one octanoate head and all other octanoate anions amounts to  $19 \pm 3 \text{ kJ mol}^{-1}$ .

Another structural change that takes place upon the association of a free monomer into a previously formed aggregate is the change in the hydration of the surfactant molecule, which must necessarily decrease during the process. Thus, the positive enthalpic contribution that we have estimated for the aggregation processes may be explained in part as resulting from the difference of the interaction energy for the anion in water compared to that for the anion inside the aggregate. The average interaction energy between the octanoate polar head and the water molecules increased from  $-510 \pm 70 \text{ kJ mol}^{-1}$  for the free monomer to  $-490 \pm 100 \text{ kJ mol}^{-1}$  for a single anion inside the aggregate. Although these figures might suggest that interaction decreased, the associated fluctuations are too large for any meaningful statistical inference to be performed based solely on the average values. These large fluctuations may be better appreciated if we inspect the interaction energy distribution for one octanoate polar head and the surrounding water molecules, taking the octanoate anion to be either in the monomeric state in the micellar solution or in the aggregated state inside the micelle. The distributions present two distinguishable populations for both states (Figure 5), with the first population being characterized by a narrower peak, which is centered at ca.  $-530 \text{ kJ mol}^{-1}$ , whereas the second population is broader and includes several lower probability states with maximum interaction energy around  $-300 \text{ kJ mol}^{-1}$ . On the basis of these histograms, the aggregation of one octanoate anion into the micellar aggregate may be pictured as being characterized by a change in the overall probability distribution of hydration patterns, as the different energies in each histogram may be ascribed to different structural motifs. The large standard deviation for the

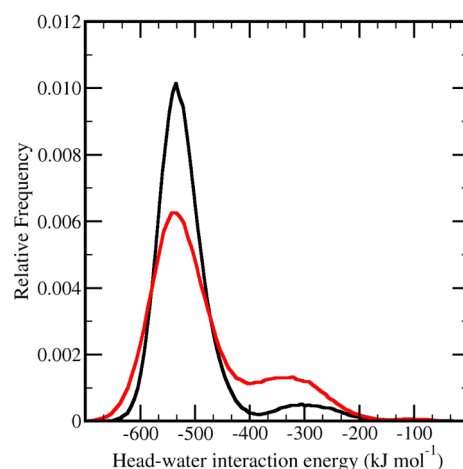


**Figure 5.** Interaction energy distribution for water and the polar head ( $\text{CH}_2\text{CO}_2^-$ ). (black solid line) One octanoate anion in solution; (red solid line) one octanoate anion inside the micelle.

interaction energy of the octanoate in the micelle compared to the monomer in solution may be due to physical phenomena that take place at the micellar aggregate but are absent for the molecule in solution, e.g., the formation of sodium ionic bridges between neighboring octanoate heads.

The structural patterns behind these energy distributions may be assessed by means of the radial distribution functions,  $g(r)$ , defined in eq 2. The population with the more negative octanoate head–water interaction energy (Figure 5) presented a larger water density in the first solvation shell compared to the population with the more positive energy for both associated octanoate and dissociated octanoate (Figure 6). One of the main differences observed for the second solvation shell was the associated octanoate anion, where the solvent structure was nearly absent for the molecules with the more positive interaction energy. Thus, we may state that the

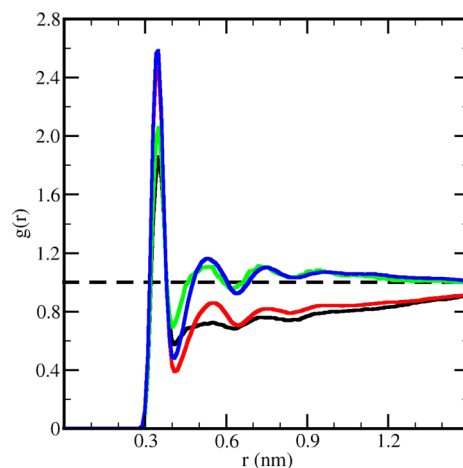


**Figure 6.** Radial distribution functions between water oxygen atoms and octanoate C1 atom, considering different interaction energies between the surfactant polar head and the surrounding water molecules. (black solid line) Energy above  $-350 \text{ kJ mol}^{-1}$  for the aggregated octanoate; (green solid line) energy above  $-350 \text{ kJ mol}^{-1}$  for the monomer in solution; (red solid line) energy below  $-500 \text{ kJ mol}^{-1}$  for the aggregated octanoate; (blue solid line) energy below  $-500 \text{ kJ mol}^{-1}$  for the monomer in solution. The dashed line stands for the ideal gas reference state.

different energy populations are correlated to different structural patterns; i.e., there are structural populations as well.

The energy distribution for the octanoate head interacting with the counterions and the histogram were computed and presented two well-defined populations (results not shown here). We might have computed the radial distribution functions for these populations, but we think it is more revealing to analyze the distribution of sodium ions around the polar headgroup for each population in Figure 5, because those correlations will provide a picture for the competition between water molecules and cations interacting with the negatively charged head. Therefore, we considered the trajectory frames for head–water energies above  $-350 \text{ kJ mol}^{-1}$  as one population and those below  $-500 \text{ kJ mol}^{-1}$  as the other. The sodium cations are not present at all in the first coordination shell around the polar heads for the population with the more negative head–water interaction, whereas a large correlation peak in the first coordination shell characterized the population with the more positive head–water interaction (Figure 7).

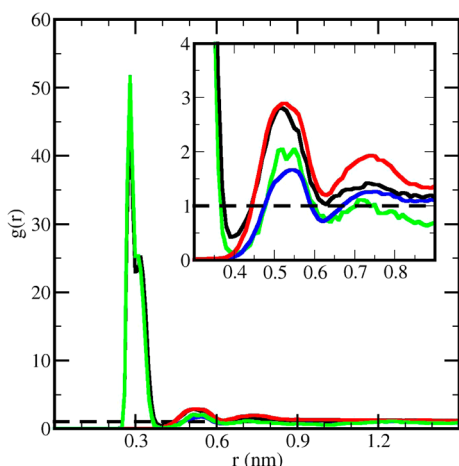


**Figure 7.** Radial distribution function between sodium counterions and octanoate C1 when the interaction energies between surfactant head and water are (black solid line) above  $-350 \text{ kJ mol}^{-1}$  and the octanoate is aggregated in the micelle, (green solid line) above  $-350 \text{ kJ mol}^{-1}$  and disaggregated, (red solid line) below  $-500 \text{ kJ mol}^{-1}$  and aggregated, and (blue solid line) below  $-500 \text{ kJ mol}^{-1}$  and disaggregated. The inset expands the region between 0.3 and 0.9 nm for better visualization of the second and the third coordination shells.

Thus, there is a continuous process of exchange in the first coordination shell around the octanoate polar heads. Whenever a sodium cation enters that region there must be some water molecules being expelled from it, and the difference in the head–water interaction energy may be ascribed to the number of water molecules comprising the first hydration shell, since we have not detected any change in the average water dipole orientation with respect to the octanoate head.

It is also interesting to note the fact that ionic bridges may be formed between neighboring octanoate ions that would otherwise be far from each other (Figure 8). This structural pattern, although rare, also affects the hydration of the polar heads, particularly at the second solvation layer, where some water molecules are replaced by the bridged anion, an effect that is not significant for the monomer in solution (Figure 6).

The positive aggregation entropic contribution of the surfactant head can be attributed, at least in part, to the partial desolvation of the octanoate head due to the micelle formation,

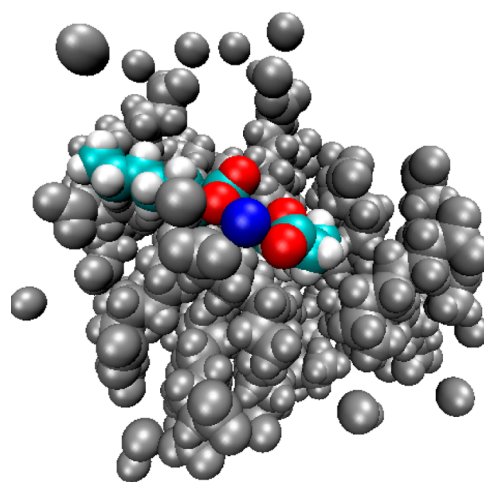


**Figure 8.** van der Waals representation of the micelle showing an ionic bridge between two octanoate ions mediated by a  $\text{Na}^+$  ion. Atoms: oxygen (red), carbon (cyan), hydrogen (light gray), and sodium (blue) for the molecules directly involved in the ionic bridge (the rest of the micelle and the counterions are represented in dark gray).

since it is well-known that the hydration entropy is negative for ions due to the strong water organization around a charged species. A secondary effect that might contribute to this positive entropic contribution is the increase in the sodium–octanoate association degree from 7% for the monomer in solution, to 22% for the octanoate in the micelle, due to the cooperative effects at the aggregate surface that are absent in the bulk solution and that might result in a further dehydration of the octanoate head and also of the associated sodium, increasing the water entropy.

**Contributions Arising from the Hydrophobic Tail.** The aliphatic tail of the octanoate anion yielded positive contributions for both the enthalpy and the entropy of aggregation. The enthalpy variation arising from the tail amounted to  $22 \pm 7 \text{ kJ mol}^{-1}$  and may be ascribed to the increase of the tail–water interaction energy from  $-50 \pm 7$  to  $-17 \pm 8 \text{ kJ mol}^{-1}$  when the octanoate is transferred from the solution into the micelle. As expected for any transfer process, the interaction lost is partially compensated for, but the interaction between the leaving/entering aliphatic tail and the other octanoate tails inside the micelle amounted to only  $-15 \pm 2 \text{ kJ mol}^{-1}$ . Although water molecules do not penetrate the micelle hydrophobic core, the tail carbon atoms are partly exposed to the surrounding aqueous solution. The hydration of the hydrophobic tails is not energetically favorable, but the molecular packing is loose due to the short chain length for the sodium octanoate (Figures 1 and 8) and may be quantitatively described by the radial distribution functions of water oxygen atoms around tail carbon atoms (Figure 9). There were correlation peaks slightly above unity for all carbon atoms belonging to the monomer in solution, whereas all correlation functions were considerably below unity for the octanoate inside the micelle. It should be pointed out that the carbon atom C2, which belongs to the first  $\text{CH}_2$  group attached to the polar head, presented a more structured correlation peak with intensity near unity, being considerably more hydrated for the aggregated surfactant compared to the other aliphatic carbon atoms. This fact gives support to the inclusion of C2 carbon into the polar head of our previous discussion about the association Gibbs energy.



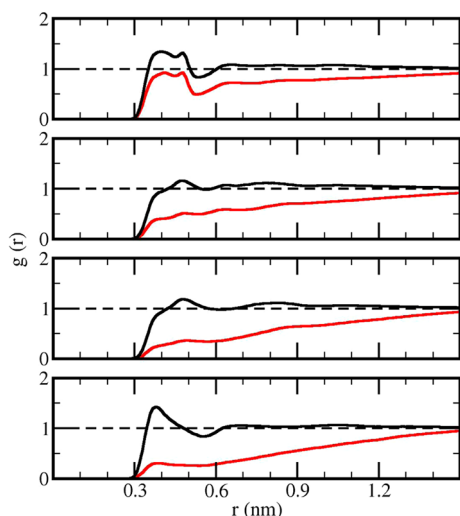


**Figure 9.** Radial distribution function of water oxygen around the carbon atoms, from top to bottom: carbon atoms 2, 4, 6, and 8 of the octanoate ion in solution (black solid line) and at the micelle (red solid line).

The histograms for the interaction energy between the tail fragment and water molecules were computed as well, for both the free octanoate in the solution and the octanoate incorporated in the micelle (Figure 10). In contrast to the

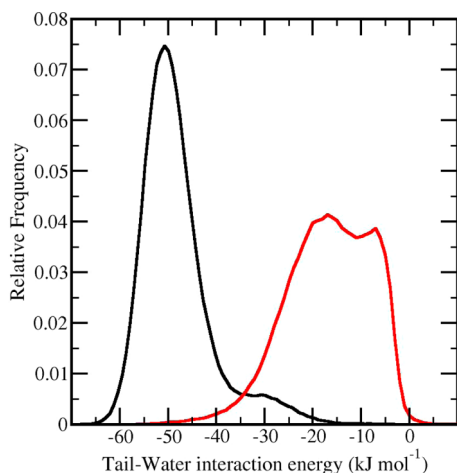


**Figure 10.** Histogram of the interaction energy between water and the tail fragment ( $\text{C}_6\text{H}_{13}$ ) of one octanoate ion in the solution (black solid line) and at the micelle (red solid line).

behavior presented by the interaction between the polar head and the water molecules, characterized by the same profile for both the free monomer and the associated surfactant, differing only by the relative probability of each energy population (Figure 5), the hydration energy profile for the tail fragment changed drastically upon aggregation, from a sharp distribution around  $-50 \text{ kJ mol}^{-1}$  to a broader distribution shifted by ca.  $30 \text{ kJ mol}^{-1}$  in the direction of more positive interaction values. These markedly different hydration energy profiles give support to the idea that not just the number of water molecules interacting with the apolar tails decreased upon micellization (Figure 9), which is reasonable, but the hydration pattern changed as well, largely favoring the less attractive interactions. This finding is in contrast to the same analysis for the head hydration energy, which changes the degree of hydration but

not the profile itself (Figure 5). Despite the great reduction of the octanoate exposition to the water solution, there was a small but significant probability of finding the hydration energy for the aggregated molecule at the same energy range of the monomer in solution, a finding that may be accounted for considering that a few octanoate tails stay aligned along the interface instead of pointing to the center of the micelle, increasing the tail exposure to the solvent (Figures 1 and 8). This finding is also consistent with the fact that a few surfactant molecules were removed from the micelle without any appreciable amount of work being expended (Figure 2).

The two populations within the hydration energy profile for the free monomer (Figure 10) may be ascribed to the different conformations of the tail: the population centered at  $-50 \text{ kJ mol}^{-1}$  corresponds to the fully extended, all-trans conformation, which presents a larger surface area exposed to the solvent, whereas the population centered at  $-30 \text{ kJ mol}^{-1}$  corresponds to the existence of gauche defects and a reduced exposition to the solvent (Figure 11).

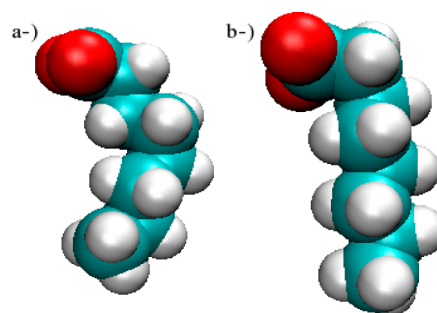


**Figure 11.** van der Waals representation of two possible conformations of octanoate ion corresponding (a) to the less negative hydration energy population for the monomer and (b) to the more negative population. Atoms: oxygen (red), carbon (cyan), and hydrogen (light gray).

The entropy increase due to the incorporation of the tail into the micelle is usually attributed to the water organization around an hydrophobic solute,<sup>14,15,19,20,45</sup> which is released in a less structured form as the surfactant becomes aggregated. The change in water organization around the surfactant tail may be estimated by means of the distribution functions describing the hydrogen bond network of the water molecules in the first hydration shell around the apolar tails in comparison with the same distributions for pure water. The distance distribution of hydrogen-bonded water molecules (Figure 12) and the angle distribution for the hydrogen bond (Figure 13) are slightly narrower for the water molecules around the octanoate methyl group compared to the same distributions in pure water. The narrower distributions are consistent with a slightly more orderly water structure around the surfactant hydrophobic tail (other aliphatic carbon atoms presented the same profiles). We should be bear in mind that this structural effect must necessarily be a slight one, since any larger perturbation should already have been characterized by spectroscopic measurements.

Another factor that is usually used to justify the positive entropy contribution of the tails to the Gibbs energy of association is allegedly the random structure of the chains inside the hydrocarbon-like core of the micelle compared to the chain conformation in the aqueous solution.<sup>45</sup> We do not consider this contribution for the sodium octanoate system, as

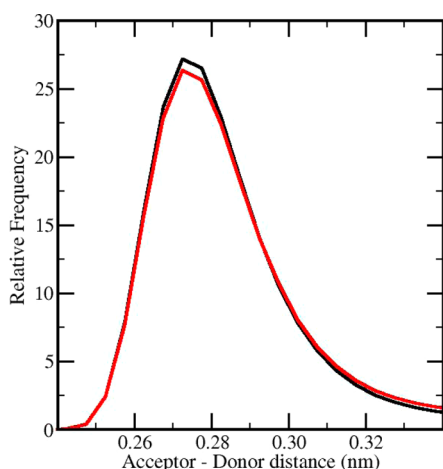


**Figure 12.** Distance distribution for the donor–acceptor oxygen atoms belonging to pairs of water molecules interacting by means of hydrogen bonds. (black solid line) Molecules within the first hydration shell around octanoate carbon atom C8 (terminal methyl group) for the monomer in solution; (red solid line) pure water distribution.

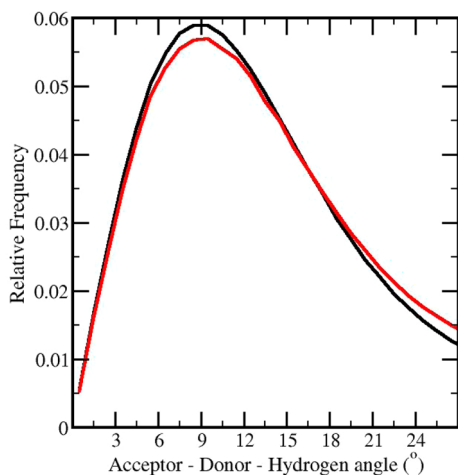


**Figure 13.** Angle distribution for the acceptor–donor–hydrogen atoms belonging to pairs of water molecules interacting by means of hydrogen bonds. (black solid line) Molecules within the first hydration shell around the octanoate carbon atom C8 (terminal methyl group) for the monomer in solution; (red solid line) pure water distribution.

we have shown in a previous work<sup>13</sup> where the dihedral distributions describing the tail conformation remained unchanged upon micellization, although the relaxation time for the dihedral transition increased. Thus, we may rule out entropy contribution arising from changes in the internal structure of the octanoate anion as being a determining factor affecting the octanoate self-assembling.

## CONCLUSIONS

The energetic and structural results arising from the molecular dynamics simulations of the sodium octanoate micellar system are consistent with the general view that the hydrophobic effect is the main contributor to micelle formation. The overall process was largely entropy-driven, as expected, but surprisingly there was a favorable entropic contribution arising from the polar head, along with the well-known favorable entropic contribution arising from the apolar tail. As a matter of fact, our

results support the idea that stable aggregates would not be observed without this contribution from the polar head.

Besides allowing the computation of the entropy contributions, the structural and energetic features arising from the molecular dynamics simulations shed some light on the origins of the thermodynamic driving forces. For instance, the entropy increase associated with water reorganization during the aggregation process may be ascribed to the structural changes observed in water molecules comprising the first hydration shell around aliphatic  $\text{CH}_2/\text{CH}_3$  groups, as characterized by the distributions of distances and angles for the hydrogen-bonded pairs. Another structural change that may produce an entropic contribution favoring the aggregation of anionic surfactants is the partial dehydration of both the charged head and bound counterions at the micelle surface. The water molecules are strongly organized within the first hydration layer around these ionic species due to the intense ion–dipole interactions and should become less orderly upon release.

On the enthalpic counterpart, the unfavorable aggregation enthalpy can be attributed to the lost hydration interactions for both the surfactant tail and head and by the electrostatic repulsion between the surfactant heads at the micellar surface. Sodium counterions may partially screen the electrostatic repulsion between the negatively charged heads, as we have observed in the case of stable ionic bridges, but most counterions remain in solution. The van der Waals interactions between the tails in the hydrophobic core are essentially attractive, but their magnitude is not large enough to compensate for the lost hydration interaction.

## AUTHOR INFORMATION

### Corresponding Author

\*E-mail: moura@ufscar.br. Tel.: +55-16-3351-8090. Fax: +55-16-3351-8350.

### Author Contributions

<sup>†</sup>The manuscript was written through contributions of all authors. All authors have given approval to the final version of the manuscript. K.B. and A.F.deM. contributed equally to this work.

### Notes

The authors declare no competing financial interest.

## ACKNOWLEDGMENTS

We thank FAPESP (2012/15147-4), CAPES, and CNPq (Brazilian funding agencies) for their financial support. We are indebted to Prof. Christopher Jarzynski for his insightful suggestions.

## REFERENCES

- (1) Pashley, R. M.; Karaman, M. E. *Applied Colloid and Surface Chemistry*; John Wiley & Sons: Chichester, U.K., 2004.
- (2) de Moura, A. F.; Freitas, L. C. G. Molecular Dynamics Simulation of the Sodium Octanoate Micelle in Aqueous Solution: Comparison of Force Field Parameters and Molecular Topology Effects on the Micellar Structure. *Braz. J. Phys.* **2004**, *34*, 64–72.
- (3) Sammalkorp, M.; Karttunen, M.; Haataja, M. Structural Properties of Ionic Detergent Aggregates: A Large-Scale Molecular Dynamics Study of Sodium Dodecyl Sulfate. *J. Phys. Chem. B* **2007**, *111*, 11722–11733.
- (4) MacKerell, A. D., Jr. Molecular Dynamics Simulation Analysis of a Sodium Dodecyl Sulfate Micelle in Aqueous Solution: Decreased Fluidity of the Micelle Hydrocarbon Interior. *J. Phys. Chem.* **1995**, *99*, 1846–1855.

- (5) Rakin, A. R.; Pack, G. R. Molecular Dynamics Simulations of Ionic Interactions with Dodecyl Sulfate Micelles. *J. Phys. Chem. B* **2004**, *108*, 2712–2716.
- (6) Wu, R.; Deng, M.; Kong, B.; Yang, X. Coarse-Grained Molecular Dynamics Simulation of Ammonium Surfactant Self-Assemblies: Micelles and Vesicles. *J. Phys. Chem. B* **2009**, *113*, 15010–15016.
- (7) Jusufi, A.; Hynninen, A. P.; Panagiotopoulos, A. Z. Implicit Solvent Models for Micellization of Ionic Surfactants. *J. Phys. Chem. B* **2008**, *112*, 13783–13792.
- (8) Marrink, S. J.; Tieleman, D. P.; Mark, A. E. Molecular Dynamics Simulation of the Kinetics of Spontaneous Micelle Formation. *J. Phys. Chem. B* **2000**, *104*, 12165–12173.
- (9) Tieleman, D. P.; van der Spoel, D.; Berendsen, H. J. C. Molecular Dynamics Simulations of Dodecylphosphocholine Micelles at Three Different Aggregate Sizes: Micellar Structure and Chain Relaxation. *J. Phys. Chem. B* **2000**, *104*, 6380–6388.
- (10) MacCallum, J. L.D.; Tieleman, D. P. Computer Simulation of the Distribution of Hexane in a Lipid Bilayer: Spatially Resolved Free Energy, Entropy, and Enthalpy Profiles. *J. Am. Chem. Soc.* **2006**, *128*, 125–130.
- (11) Tieleman, D. P.; Marrink, S. J. Lipids out of Equilibrium: Energetics of Desorption and Pore Mediated Flip-Flop. *J. Am. Chem. Soc.* **2006**, *128*, 12462–12467.
- (12) Widge, A. S.; Matsuo, Y.; Kurnikova, M. Computational Modeling of Poly(alkylthiophene) Conductive Polymer Insertion into Phospholipid Bilayers. *Langmuir* **2007**, *23*, 10672–10681.
- (13) de Moura, A. F.; Bernardino, K.; de Oliveira, O. V.; Freitas, L. C. G. Solvation of Sodium Octanoate Micelles in Concentrated Urea Solution Studied by Means of Molecular Dynamics Simulations. *J. Phys. Chem. B* **2011**, *115*, 14582–14590.
- (14) Tanford, C. *The Hydrophobic Effect: Formation of Micelles and Biological Membranes*, 2nd ed.; Wiley: New York, 1980.
- (15) Butler, J. A. V. The Energy and Entropy of Hydration of Organic Compounds. *Trans. Faraday Soc.* **1937**, *33*, 229–236.
- (16) del Rio, J. M.; Jones, M. N. Thermodynamics of the Hydrophobic Effect. *J. Phys. Chem. B* **2001**, *105*, 1200–1211.
- (17) Huang, D. M.; Chandler, D. The Hydrophobic Effect and the Influence of Solute–Solvent Attractions. *J. Phys. Chem. B* **2002**, *106*, 2047–2053.
- (18) Solomonov, B. N.; Sedov, I. A. Quantitative Description of the Hydrophobic Effect: The Enthalpic Contribution. *J. Phys. Chem. B* **2006**, *110*, 9298–9303.
- (19) Southall, N. T.; Dill, K. A. The Mechanism of Hydrophobic Solvation Depends on Solute Radius. *J. Phys. Chem. B* **2000**, *104*, 1326–1331.
- (20) Frank, H. S.; Evans, M. W. Free Volume and Entropy in Condensed Systems III. Entropy in Binary Liquid Mixtures; Partial Molal Entropy in Dilute Solutions; Structure and Thermodynamics in Aqueous Electrolytes. *J. Chem. Phys.* **1945**, *13*, 507–532.
- (21) Lei, Y.; Leng, Y. Hydrophobic Drying and Hysteresis at Different Length Scales by Molecular Dynamics Simulations. *Langmuir* **2012**, *28*, 3152–3158.
- (22) Maiti, M.; Weiner, S.; Buldyrev, S. V.; Stanley, E.; Sastry, S. Potential of Mean Force between Hydrophobic Solutes in the Jagla Model of Water and Implications for Cold Denaturation of Proteins. *J. Chem. Phys.* **2012**, *136*, 044512–1–044512–7.
- (23) Rosenholm, J. B. The Structure and Properties of Medium-Chain Surfactant Solutions: A Case Study of Sodium Octanoate. *Adv. Colloid Interface Sci.* **1992**, *41*, 197–239.
- (24) Harvey, S. C.; Prabhakaran, M. Umbrella Sampling: Avoiding Possible Artifacts and Statistical Biases. *J. Phys. Chem.* **1987**, *91*, 4799–4801.
- (25) Hill, T. L. *An Introduction to Statistical Thermodynamics*; Dover Publications, Inc.: New York, 1986.
- (26) Ferrenberg, A. M.; Swendsen, R. H. Optimized Monte Carlo Data Analysis. *Phys. Rev. Lett.* **1989**, *63*, 1195–1198.
- (27) Kumar, S.; Bouzida, D.; Swendsen, R. H.; Kollman, P. A.; Rosenberg, J. M. The Weighted Histogram Analysis Method for Free-Energy Calculations on Biomolecules. *J. Comput. Chem.* **1992**, *13*, 1011–1021.
- (28) Zhu, F.; Hummer, G. Convergence and Error Estimation in Free Energy Calculations Using the Weighted Histogram Analysis Method. *J. Comput. Chem.* **2012**, *33*, 453–465.
- (29) Jarzynski, C. Nonequilibrium Equality for Free Energy Differences. *Phys. Rev. Lett.* **1997**, *78*, 2690–2693.
- (30) Neumann, R. M. Entropic approach to Brownian Movement. *Am. J. Phys.* **1980**, *48*, 354–357.
- (31) van der Spoel, D.; Lindahl, E.; Hess, B.; and the GROMACS development team. *GROMACS User Manual*, version 4.6.1; 2013. [www.gromacs.org](http://www.gromacs.org).
- (32) Berendsen, H. J. C.; van der Spoel, D.; van Drunen, R. GROMACS: A Message-Passing Parallel Molecular Dynamics Implementation. *Comput. Phys. Commun.* **1995**, *91*, 43–56.
- (33) Lindahl, E.; Hess, B.; van der Spoel, D. GROMACS 3.0: A Package for Molecular Simulation and Trajectory Analysis. *J. Mol. Model.* **2001**, *7*, 306–317.
- (34) van der Spoel, D.; Lindahl, E.; Hess, B.; Groenhof, G.; Mark, A. E.; Berendsen, H. J. C. GROMACS: Fast, Flexible, and Free. *J. Comput. Chem.* **2005**, *26*, 1701–1718.
- (35) Jorgensen, W. L.; Maxwell, D. S.; Tirado-Rives, J. Development and Testing of the OPLS All-Atom Force Field on Conformational Energetics and Properties of Organic Liquids. *J. Am. Chem. Soc.* **1996**, *118*, 11225–11236.
- (36) Åqvist, J. Ion–Water Interaction Potentials Derived from Free Energy Perturbation Simulations. *J. Phys. Chem.* **1990**, *94*, 8021–8024.
- (37) Berendsen, H. J. C.; Postma, J. P. M.; van Gusteren, W. F.; Hermans, J. In *Intermolecular Forces*; Pullman, B., Ed.; Reidel: Dordrecht, 1981.
- (38) Darden, T.; York, D.; Pedersen, L. Particle Mesh Ewald: An N-log(N) Method for Ewald Sums in Large Systems. *J. Chem. Phys.* **1993**, *98*, 10089–10092.
- (39) Essmann, U.; Perera, L.; Berkowitz, M. L.; Darden, T.; Lee, H.; Pedersen, L. G. A Smooth Particle Mesh Ewald Method. *J. Chem. Phys.* **1995**, *103*, 8577–8593.
- (40) Berendsen, H. J. C.; Postma, J. P. M.; DiNola, A.; Haak, J. R. Molecular Dynamics with Coupling to an External Bath. *J. Chem. Phys.* **1984**, *81*, 3684–3690.
- (41) Humphrey, W.; Dalke, A.; Schulten, K. VMD—Visual Molecular Dynamics. *J. Mol. Graphics* **1996**, *14* (1), 33–38.
- (42) Davies, J. T. A Quantitative Kinetic Theory of Emulsion Type. I. Physical Chemistry of the Emulsifying Agent. *Proceedings of the Second International Congress of Surface Activity*; Butterworths: London, 1957; pp 426–438.
- (43) Myers, D. *Surfaces, Interfaces and Colloids. Principles and Applications*, 2nd ed.; John Wiley & Sons: New York, 1999.
- (44) Hunter, R. J. *Foundations of Colloid Science*; Oxford University Press: Oxford, 2001.
- (45) Israelachvili, J. N. *Intermolecular and Surface Forces*, 2nd ed.; Academic Press: London, 1998.